

Global Stability of Three-dimensional Disturbances in Blasius Boundary-layer Flow over a Compliant Panel

K. Tsigklifis¹ and A. D. Lucey¹

¹Fluid Dynamics Research Group
 Department of Mechanical Engineering
 Curtin University, Perth, WA 6845, Australia

Abstract

A hybrid of computational and theoretical approaches is developed to model the interaction of a Blasius boundary-layer flow interacting with a compliant panel that is embedded in an otherwise rigid flat plate. The study is motivated by the potential of compliant panels to reduce the amplification of Tollmien-Schlichting waves (TSWs) as a means to control boundary-layer transition. Using a classical decomposition into mean and perturbation quantities of the system variables, the velocity-vorticity forms of the three-dimensional Navier-Stokes equations are solved after linearisation. The compliant panel is modelled using classical thin-plate theory added to which is a spring foundation. Flow and wall mechanics are then fully coupled and a fluid-structure interaction (FSI) system eigen-problem is assembled. Results show that global instabilities may occur when either of a TSW or a wall-based instability called travelling-wave flutter (TWF) couples with a structural mode. The compliant panel reduces the spatial amplification of convectively unstable TSWs although the finite width of the panel, as modelled by spanwise variation of the mode, decreases this beneficial effect. However, the effect of the panel width on the globally unstable TWF-type mode is strongly stabilising. Overall the results indicate that panel aspect ratio in the three-dimensional FSI system will be an important parameter in the design of practicable compliant panels for drag reduction.

Introduction

It is well known that compliant walls are able to reduce the growth rates of Tollmien-Schlichting waves (TSWs) in marine applications. This has, for example, been demonstrated theoretically in [1] and confirmed experimentally in [6]. Conventional transition via the amplification of TSWs can therefore be postponed through the use of compliant coatings adhered to an otherwise rigid surface. The extension of the laminar boundary-layer region can then yield a reduction to skin-friction drag. However, compliant walls have also been shown to support hydro-elastic instabilities such as divergence and travelling-wave flutter (TWF) [9, 11] that can trigger premature transition and thus for a practicable technology these must be accounted for the choice of the compliant coating. To date, optimisations of compliant-wall performance have been based upon two-dimensional (2D) local analyses; for example see [2, 4].

Local spatial stability studies of three-dimensional (3D) disturbances [16, 7] and DNS [14] have shown that 3D TSW modes over compliant coatings may be more dominant than their 2D counterparts because there is an apparent increase in panel stiffness (relative to the free-stream dynamic pressure) in their direction of propagation. However, this effect is beneficial with respect to the hydro-elastic instabilities as is the side-edge restraint as shown, for example, in [10]. A recent global stability analysis of 2D disturbances [13] takes into account compliant-wall boundary conditions and predicts that interaction-resonance between the panel and the TWF or TSW

modes can take place rendering the system globally unstable with temporal growth.

In this paper we develop solutions to the linearised three-dimensional velocity-vorticity formulation of [3] using a boundary-integral method based on the generalized Helmholtz decomposition of the flow field [8, 15]. These are fully coupled to the linear dynamics of a 2D orthotropic Kirchhoff plate. Herein we use the model to determine time-asymptotic global stability of the FSI system through the extraction of a significant part of the eigen-spectrum. However, the model could equally be used to undertake the transient analysis through integration in time of the system model.

Theoretical and Computational Modelling

Mean Flow Field

The mean flow of interest is the zero-pressure-gradient flat-plate boundary layer; see figure 1. The displacement thickness δ'_s at

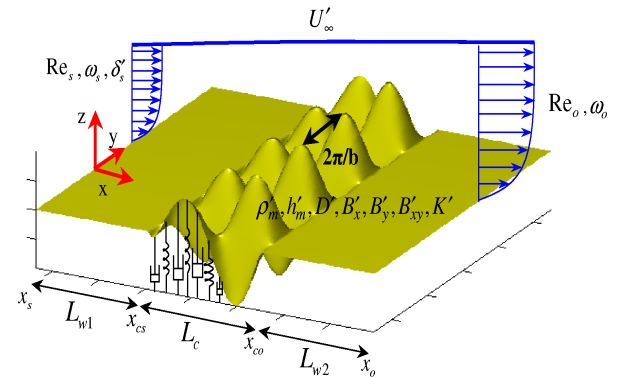


Figure 1: Schematic of the system studied with nomenclature

the entrance x'_s of the flow field is assigned as the characteristic length scale, while the free-stream flow speed wholly in the x -direction is U'_∞ is used as the characteristic velocity, where primes denote dimensional quantities. The local Reynolds number, Re_x , at position x of the flow field is related to the Re_s at the entrance of the domain through, $Re_x = \gamma(xRe_s)^{1/2}$, where $Re_s = \rho'_l U'_\infty \delta'_s / \mu'_l = \gamma(\rho'_l U'_\infty x'_s / \mu'_l)^{1/2}$ and $\gamma = 1.7208$ for the Blasius profile. The undisturbed streamwise and vertical velocity components in the growing boundary layer are respectively defined by, $U_x = df/dH$ and $U_z = (\gamma/2)(xRe_s(H(df/dH) - f))^{1/2}$, where $f(H)$ satisfies the Blasius equation,

$$2 \frac{d^3 f}{dH^3} + \gamma^2 f \frac{d^2 f}{dH^2} = 0, \quad (1)$$

in which with $H = z/(\gamma\sqrt{x/Re_s})$ subject to the boundary conditions $f(0) = [df/dH](0) = 0$ and $df/dH \rightarrow 0$ as $H \rightarrow \infty$.

Disturbance Field

Starting from the general velocity-vorticity disturbance formulation found in [3], allowing 3D disturbances and retaining only the linear velocity and vorticity terms, we obtain the following equations for the disturbances:

$$\begin{aligned} \frac{\partial \omega_x}{\partial t} - \Omega_y \frac{\partial u_x}{\partial y} + U_x \frac{\partial \omega_x}{\partial x} - \frac{\partial U_x}{\partial z} \omega_z + U_z \frac{\partial \omega_x}{\partial z} + \frac{\partial U_z}{\partial z} \omega_x \\ = \frac{1}{Re_s} \left(\frac{\partial^2 \omega_x}{\partial x^2} + \frac{\partial^2 \omega_x}{\partial y^2} + \frac{\partial^2 \omega_x}{\partial z^2} \right), \end{aligned} \quad (2)$$

$$\begin{aligned} \frac{\partial \omega_y}{\partial t} - \Omega_y \frac{\partial u_y}{\partial y} + \frac{\partial \Omega_y}{\partial x} u_x + \frac{\partial \Omega_y}{\partial z} u_z + U_x \frac{\partial \omega_y}{\partial x} + U_z \frac{\partial \omega_y}{\partial z} \\ = \frac{1}{Re_s} \left(\frac{\partial^2 \omega_y}{\partial x^2} + \frac{\partial^2 \omega_y}{\partial y^2} + \frac{\partial^2 \omega_y}{\partial z^2} \right), \end{aligned} \quad (3)$$

with variables of the mean Blasius flow assigned capital letters and those of the disturbances are in lowercase and noting x , y and z are respectively, the streamwise, spanwise and vertical coordinates. Following [3], we solve equations (2) and (3) together with the integral representation in the vertical direction of the definition of spanwise and the streamwise vorticity respectively, and the vorticity continuity written as follows:

$$u_x = - \int_z^\infty \left(\omega_y + \frac{\partial u_x}{\partial x} \right) dz, \quad (4)$$

$$u_y = \int_z^\infty \left(\omega_x - \frac{\partial u_x}{\partial y} \right) dz, \quad (5)$$

$$\omega_z = \int_z^\infty \left(\frac{\partial \omega_x}{\partial x} + \frac{\partial \omega_y}{\partial y} \right) dz. \quad (6)$$

Instead of solving the normal (to the flow) component of the vector Poisson equation, we employ a Helmholtz decomposition, [15, 8], and couch the disturbance flow field as the sum of its rotational and an irrotational velocity fields. Then, the normal component of the velocity field can be expressed as an integral representation of the streamwise and spanwise vorticity in the domain and of a prescribed normal velocity on the boundary, \hat{u}_{zB} ; thus

$$\begin{aligned} \hat{u}_z(x'', z'') &= - \int_0^\infty \int_{x_s}^{x_o} \hat{\omega}_y(x, z) \frac{\partial G(x, z, x'', z'')}{\partial x} dx dz, \\ &- \int_0^\infty \int_{x_s}^{x_o} i \cdot b \cdot \hat{\omega}_x(x, z) G(x, z, x'', z'') dx dz, \\ &- \int_{x_s}^{x_o} \left[\hat{u}_{zB}(x) \frac{\partial G(x, z, x'', z'')}{\partial z} \right]_{z=0}^{z=\infty} dx, \\ &- \int_0^\infty \left[\hat{u}_{zB}(z) \frac{\partial G(x, z, x'', z'')}{\partial x} \right]_{x=x_s}^{x=x_o} dz, \end{aligned} \quad (7)$$

where $G = (1/(2\pi))K_0(b\sqrt{(x''-x)^2 + (z''-z)^2})$ is the screened quasi-2D Green's function, K_0 is the zero-th order modified Bessel function of the second kind and b is the disturbance wavenumber in the spanwise direction. In the above integral expression \hat{u}_{zB} is determined by the imposition of boundary condition, namely the normal velocity on the wall and at infinity, and the streamwise gradients of the normal velocity at the entrance and exit of the domain.

Structural Solution

We use the 2D orthotropic Kirchhoff plate equation with additional terms to account for a dashpot-type damping and a uniformly distributed spring foundation. Thus, vertical displacements of the plate, $\eta(x, y, t)$, with the non-dimensionalised (by free-stream dynamic pressure) perturbation-pressure loading, $p(x, y, 0, t)$, at the (linearised) plate-fluid interface are governed by

$$\begin{aligned} -p(x, y, 0, t) &= M \frac{\partial^2 \eta}{\partial t^2} + D \frac{\partial \eta}{\partial t} + K \cdot \eta \\ &+ B_x \frac{\partial^4 \eta}{\partial x^4} + 2B_{xy} \frac{\partial^4 \eta}{\partial x^2 \partial y^2} + B_y \frac{\partial^4 \eta}{\partial y^4} \end{aligned} \quad (8)$$

where the non-dimensional coefficients of inertia, damping, spring-foundation stiffness, flexural rigidity in the streamwise, cross and spanwise direction respectively, are defined by

$$\begin{aligned} M &= \frac{\rho'_m h'_m}{\rho'_f \delta'_s}, \quad D = \frac{D'}{\rho'_f U_\infty}, \quad K = \frac{K' \delta'_s}{\rho'_f U_\infty^2}, \\ B_x &= \frac{B'_x}{\rho'_f U_\infty^2 \delta'_s{}^3}, \quad B_{xy} = \frac{B'_{xy}}{\rho'_f U_\infty^2 \delta'_s{}^3}, \quad B_y = \frac{B'_y}{\rho'_f U_\infty^2 \delta'_s{}^3}. \end{aligned}$$

Hinged boundary conditions are applied at the leading and trailing edges of the compliant wall, hence

$$\begin{aligned} \eta(x_{cs}, y, t) &= \eta(x_{co}, y, t) = 0, \\ \frac{\partial^2 \eta}{\partial x^2}(x_{cs}, y, t) &= \frac{\partial^2 \eta}{\partial x^2}(x_{co}, y, t) = 0 \end{aligned} \quad (9)$$

Boundary Conditions

Following [5], we make use of the Robin boundary conditions at the entrance x_s and exit x_o of the fluid domain

$$\frac{\partial \omega_x}{\partial x} = i\alpha \omega_x, \quad \frac{\partial \omega_y}{\partial x} = i\alpha \omega_y, \quad \frac{\partial u_x}{\partial x} = i\alpha u_x \quad (10)$$

where the complex wavenumber α is the solution of the Orr-Sommerfeld equation at the entrance and at the exit of the fluid domain for real cyclical frequencies ω_s and $\omega_o = (Re_o/Re_s)\omega_s$, respectively and for real spanwise wavenumber b .

The rigid-wall boundary conditions are $u_x(x, y, 0, t) = u_y(x, y, 0, t) = u_z(x, y, 0, t) = 0$. Over the compliant-wall section the velocity and stress components are matched between fluid and solid; Thus, the linearized velocity-component boundary conditions for $x_{cs} \leq x \leq x_{co}$ are

$$u_x(x, y, 0, t) + \eta(x, y, t) \frac{\partial U_x}{\partial z}(x, y, 0, t) = 0 \quad (11)$$

$$u_y(x, y, 0, t) = 0 \quad (12)$$

$$u_z(x, y, 0, t) = \frac{\partial \eta}{\partial t}(x, y, t) \quad (13)$$

The pressure perturbation on the wall is obtained by integrating the linearized z -momentum equation between the wall and infinity where it must vanish; thus

$$\begin{aligned} p(x, y, 0, t) &= \int_0^{L_H} \left(\frac{\partial u_x}{\partial t} \right) \gamma \sqrt{\frac{x}{Re_s}} dH \\ &+ \int_0^{L_H} \left(\frac{\partial U_x}{\partial x} u_x + \frac{\partial U_x}{\partial z} u_z \right) \gamma \sqrt{\frac{x}{Re_s}} dH \\ &+ \int_0^{L_H} \left(U_x \frac{\partial u_x}{\partial x} + U_z \frac{\partial u_x}{\partial z} \right) \gamma \sqrt{\frac{x}{Re_s}} dH \\ &+ \int_0^{L_H} \frac{1}{Re_s} \left(\frac{\partial \omega_y}{\partial x} - \frac{\partial \omega_x}{\partial y} \right) \gamma \sqrt{\frac{x}{Re_s}} dH \end{aligned} \quad (14)$$

where, L_H is the total height of domain, made large enough to ensure that all disturbances vanish there. Thus at $z = L_H$, $\omega_x = \omega_y = u_z = 0$ and $u_x = u_y = \omega_z = 0$. The first three conditions are imposed directly to equations (2), (3) and (7), while the second three are implicitly imposed through equations (4), (5) and (6).

Eigenvalue Form

We proceed by applying the decomposition,

$$K(x, y, z, t) = \hat{K}(x, z) e^{i b y} e^{\lambda t} + c.c., \quad (15)$$

with $\lambda = -i\omega$ and $c.c.$ the complex conjugate, to the linear system of equations (2) - (6) taking into account the integral equation (7) and the boundary conditions and transform the system equations to the generalized eigenvalue problem

$$[C_2] \{ \hat{X} \} = \lambda [C_1] \{ \hat{X} \}, \quad \{ \hat{X} \} = \{ \hat{\omega}_x, \hat{\omega}_y, \hat{u}_{zB}, \hat{\eta}, \hat{\phi} \}^T, \quad (16)$$

where $\hat{\phi} = \lambda \hat{\eta}$, from which the eigenvalues λ and eigenvectors $\{\hat{X}\}$ can be extracted. If the real part of an eigenvalue λ is positive, instability in time is predicted, otherwise the disturbances decay with time. It is remarked that the system equation (16) is of a lower order than that which would ensue if the Poisson equation were used since in the present method \hat{u}_{zB} is evaluated only on the boundary.

Numerical Solution

A fourth-order finite-difference method is used for discretisation in the streamwise direction and a Chebyshev pseudospectral method is exploited for the normal direction, noting that discretisation is not required in the spanwise direction due to the modal decomposition applied in equation (15). The flow domain is divided into $M = M_{w1} + M_c + M_{w2}$ elements in the streamwise direction, where M_{w1} , M_c and M_{w2} are the number of fluid cells over rigid-wall 1, the compliant-wall and rigid-wall 2 sections respectively, while $N+1$ points are used in the normal direction for which a linear transformation is used that maps the collocation points between the interval $[1, 0]$ and $[0, L_H]$ in the physical domain.

The Helmholtz decomposition, equation (7), is approximated by zero-order vortex sheets and zero-order source sheets. When the source point \vec{x}'' coincides with a field point, \vec{x} , the Green's function in the second integral of equation (7) exhibits a logarithmic singularity and logarithmic Gauss integration is used for the integral calculation instead of Gauss-Legendre. The trapezoidal rule is used for the calculation of the integrals in expressions (4) - (6) and (14). Finally, the Arpack library is used to extract a significant part of the spectrum of equation (16), namely 3000 eigenvalues and their respective eigenvectors, using a relatively large Krylov subspace of 9000 vectors.

Results

In the present paper we focus on the global stability of system modes arising from each of the well-known travelling-wave flutter (TWF) and Tollmien-Schlichting Waves (TSWs) predicted to occur in Blasius boundary-layer flow over compliant walls using local and global stability analyses of 2D disturbances [13]. Accordingly, we choose the wall parameters in such a way that the numerically calculated critical velocity for the onset of the divergence instability in potential flow over a finite compliant wall [12] is well above the free-stream velocity $U_\infty^l = 10m/s$ used herein. Throughout the results, the fluid is water with density $\rho_l^l = 1000kg/m^3$ and dynamic viscosity $\mu_l^l = 1.37 \times 10^{-3} Ns/m$ and the Reynolds number at the entrance to the domain, Re_s , set to 3000 where we set $\omega_s = 0.07755$. The spanwise wavenumber b was set to 0.05 and 0.1 in order to assess the effect of the transverse disturbance wavelength on the aforementioned instabilities. The isotropic compliant panel was chosen to be of Kramer-type [1] with flexural rigidity, spring coefficient, thickness and density, $B'_x = B'_y = B'_{xy} = 8.89 \times 10^{-6} Nm$, $K' = 115 \times 10^6 N/m^3$, $h'_m = 2 \times 10^{-3} m$ and $\rho'_m = 1000 kg/m^3$, respectively. Finally, the length of the upstream and downstream rigid walls were chosen to be $L'_{w1} = L'_{w2} = 0.01 m$ and the length of the compliant panel was $L'_c = 0.04 m$.

Figure 2 shows the frequency eigen-spectrum of the FSI system at spanwise wavenumber $b = 0.05$ for three levels of discretisation; convergence of the solution for a 150×65 mesh can be deduced for the eigenfrequencies close to the real axis with the exception of a branch in the range $\omega_r > 0.25$ and $\omega_i < 0$ that is a numerical artefact; this occurs for very low transverse wavenumbers and arises because the kernel K_0 and, even more intensely its derivatives, become singular as $b \rightarrow 0$. As in the corresponding 2D analysis of system disturbances, [13],

the eigen-spectrum consists of a variety of wave-type branches. Depending on the position of the fluid-loaded structural modes in the frequency spectrum, they can extract mean-flow energy through resonance either with the wall-based TWF (M_2 branch) convective instabilities - seen in figure 2 as $\omega_i > 0$ - or the fluid based TSWs (M_1 branch) - not seen in figure 2 for these wall-flow properties - giving rise to global instabilities in time. The isolated temporally unstable mode (M_3) seen in figure 2 is associated with the inlet boundary condition and is stable in space (not shown). Figure 3, shows the frequency spectrum

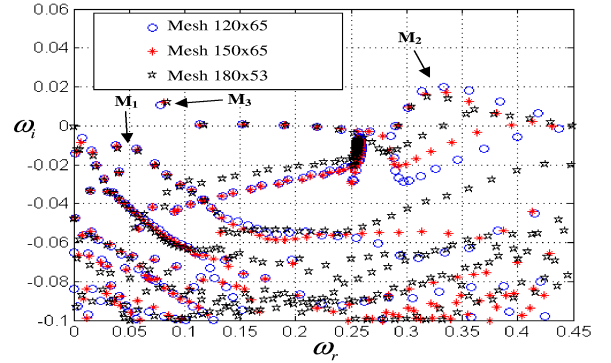


Figure 2: ω -plane eigenvalue spectrum of the FSI system for spanwise wavenumber $b = 0.05$ with three levels of discretisation

for both the compliant-wall and rigid-wall systems for $b = 0.05$ and 0.1. Note that the rigid-wall cannot support the TWF-type modes (M_2 branch labelled in figure 2). For the TSW modes (M_1 branch) that occur over both compliant and rigid walls it is seen - as denoted by the arrows - that the larger spanwise wavelength disturbance ($b = 0.05$) is less stable in time than that with the smaller spanwise wavelength ($b = 0.1$), thereby reinforcing the notion, based upon Squire's theorem, that 2D flow-aligned TSWs are the most unstable in Blasius boundary-layer flow over rigid or relatively stiff compliant walls (as is the case for the properties used to generate figure 3). Wall-compliance generally has a temporally stabilizing effect on the modes with higher frequency ($\omega_r > 0.08$) than those of the least stable TSW modes, while in the lower frequency spectrum ($\omega_r < 0.08$) compliance is destabilizing.

However, the most prominent and important feature of the high-frequency range of figure 3 is the globally unstable TWF-type mode. For this temporal instability it is seen that decreasing the transverse wavelength (from wavenumber $b = 0.05$ to 0.1) - that would be forced by a compliant panel of finite width - has a strong stabilising effect on the instability. This result supports the prevailing idea that the mechanism for TWF is primarily two-dimensional. While figures 2 and 3 show that the TSW mode is globally stable, it remains convectively unstable. In order to assess the effect of the compliant panel and of the spanwise wavelength on its growth as it propagates downstream, we plot in figure 4, the spatial amplification of the least stable TSW mode; this is achieved by computing the evolution of normalised kinetic energy of the wave as it travels downstream. Comparing the compliant- and rigid-walled systems at the corresponding transverse wavenumbers, it is seen that compliance does work to reduce the spatial amplification of TSWs. In addition, the compliant panels of finite width become more effective in reducing the amplitude of TSWs of smaller spanwise wavelength.

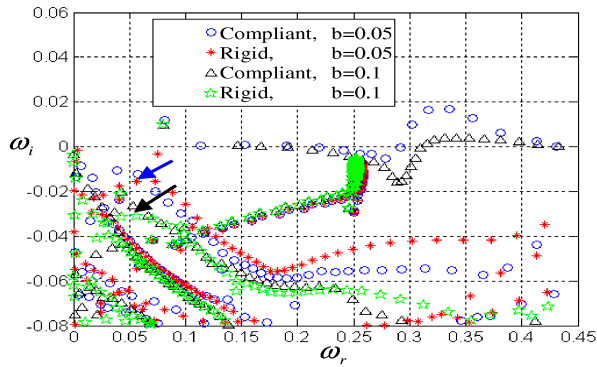


Figure 3: ω -plane eigenvalue spectrum of the compliant-wall and rigid-wall systems, each for different values of the spanwise wavelength disturbance

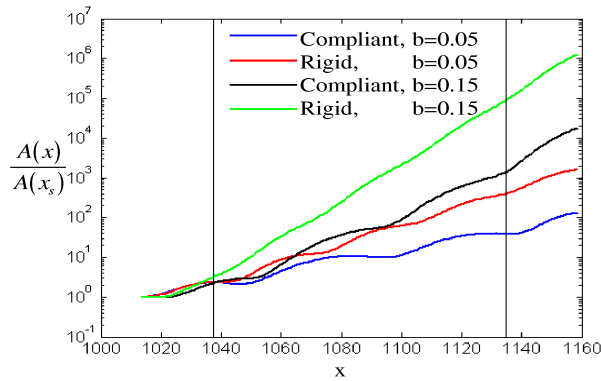


Figure 4: Spatial amplifications of the TSW modes shown in figure 3 with blue and black arrows. The vertical lines signify the leading and trailing edge of the compliant panel

Conclusions

This paper has presented a method for the analysis of the global stability of 3D disturbances in Blasius boundary-layer flow over a compliant panel in the transitional range of Reynolds number. A significant advantage of the present formulation and its solution is the reduction of the number of system variables through the use of a boundary-integral method that effectively solves the Poisson equation in the direction normal to the flow. The illustrative results presented show that the compliant panel exerts a strong stabilising effect on the spatial amplification of 3D TSWs and this beneficial effect becomes bigger for smaller spanwise wavelengths. Globally unstable TWF-type waves are also predicted and it is shown that three-dimensional effects significantly reduce their temporal growth rate. In addition, based on the non-monotonic effect of the compliant wall on the temporal stabilization of the eigenfrequencies, the transient growth over a compliant wall may play a non-trivial role; confirmation of this is left to a future work using the present system model.

Acknowledgements

The authors gratefully acknowledge the support of the Australian Research Council for the present work through the support of Discovery grant DP1096376.

References

[1] Carpenter, P.W. and Garrad, A.D., The hydrodynamic stability of flows over Kramer-type compliant surfaces: Part

1. Tollmien-Schlichting instabilities. *Journal of Fluid Mechanics*, **155**, 1985, 465–510.

[2] Carpenter, P.W., Davies, C. and Lucey, A.D., Hydrodynamics and compliant walls: Does the dolphin have a secret? *Current Science*, **79**(3), 2000, 758–765.

[3] Davies, C. and Carpenter, P.W., A novel velocity-vorticity formulation of the Navier-Stokes equations with applications to boundary layer disturbance evolution. *Journal of Computational Physics*, **172**, 2001, 119–165.

[4] Dixon, A.E., Lucey, A.D. and Carpenter, P.W., The optimization of viscoelastic walls for transition delay. *AIAA Journal*, **32**, 1994, 256–267.

[5] Ehrenstein, U. and Gallaire, F., On two-dimensional temporal modes in spatially evolving open flows: the flat-plate boundary layer. *Journal of Fluid Mechanics*, **536**, 2005, 209–218.

[6] Gaster, M., Is the dolphin a red herring? *Proceedings of the IUTAM Symposium on Turbulent Management and Relaminarization*, Bangalore, India (editors: H.W. Liepmann and R.Narasimha), Berlin: Springer, 1987, 285–304.

[7] Joslin R.D., Morris P.J. and Carpenter P.W., The role of three-dimensional instabilities in compliant wall boundary-layer transition. *AIAA Journal*, **29**, 1991, 1603–1610.

[8] Kempka, S.N., Strickland J.H., Glass M.W., Peery J.S. and Ingber M.S., Velocity boundary conditions for vorticity formulations of the incompressible Navier-Stokes equations. *Forum on vortex methods for engineering applications*, sponsored by Sandia National Labs, Albuquerque, NM, 1995, 1–22.

[9] Lucey, A.D. and Carpenter, P.W., A numerical simulation of the interaction of a compliant wall and inviscid flow. *Journal of Fluid Mechanics*, **234**, 1992, 121–146.

[10] Lucey, A.D. and Carpenter, P.W., The Hydroelastic Stability of Three-Dimensional Disturbances of a Finite Compliant Wall. *Journal of Sound and Vibration*, **165**(3), 1993, 527–552

[11] Lucey, A.D. and Carpenter, P.W., Boundary layer instability over compliant walls: Comparison between theory and experiment. *Physics of Fluids*, **7**(10), 1995, 2355–2363.

[12] Pitman, M. W. and Lucey, A. D., On the direct determination of the eigenmodes of finite flow-structure systems. *Proceedings of the Royal Society A*, **465**, 2009, 257–281.

[13] Tsigklifis, K. and Lucey, A.D., Stability of Blasius Boundary layer flow interacting with a compliant panel. *Proceedings of the ASME 2014 PVP Conference*, Anaheim, California, USA, 2014

[14] Wang, Z., Yeo, K.S. and Khoo, B.C., Spatial direct numerical simulation of transitional boundary layer over compliant surfaces. *Computers and Fluids*, **34**, 2005, 1062–1095.

[15] Wu, J.C. and Thompson, J.F., Numerical solutions of time-dependent incompressible Navier-Stokes equations using an integro-differential formulation. *Computers and Fluids*, **1**, 1973, 197–215.

[16] Yeo, K.S., The three-dimensional stability of boundary-layer flow over compliant walls. *J. Fluid Mech.*, **238**, 1992, 537–577.